Atmospheric Environment 48 (2012) 152–164

Contents lists available at ScienceDirect

Atmospheric Environment

journal homepage: www.elsevier.com/locate/atmosenv

A study of the arrival over the United Kingdom in April 2010 of the Eyjafjallajökull ash cloud using ground-based lidar and numerical simulations

B.J. Devenish [a,*], D.J. Thomson [a], F. Marenco [a], S.J. Leadbetter [a], H. Ricketts [b], H.F. Dacre [c]

[a] Met Office, FitzRoy Road, Exeter EX1 3PB, UK
[b] School of Earth, Atmospheric and Environmental Sciences, University of Manchester, Manchester M13 9PL, UK
[c] Department of Meteorology, University of Reading, Earley Gate, PO Box 243, Reading RG6 6BB, UK

ARTICLE INFO

Article history:
Received 7 February 2011
Received in revised form
10 June 2011
Accepted 13 June 2011

Keywords:
Atmospheric dispersion
Lidar
Volcanic ash

ABSTRACT

We make a qualitative and quantitative comparison of numerical simulations of the ash cloud generated by the eruption of Eyjafjallajökull in April 2010 with ground-based lidar measurements at Exeter and Cardington in southern England. The numerical simulations are performed using the Met Office's dispersion model, NAME (Numerical Atmospheric-dispersion Modelling Environment). The results show that NAME captures many of the features of the observed ash cloud. The comparison enables us to estimate the fraction of material which survives the near-source fallout processes and enters into the distal plume. A number of simulations are performed which show that both the structure of the ash cloud over southern England and the concentration of ash within it are particularly sensitive to the height of the eruption column (and the consequent estimated mass emission rate), to the shape of the vertical source profile and the level of prescribed 'turbulent diffusion' (representing the mixing by the unresolved eddies) in the free troposphere with less sensitivity to the timing of the start of the eruption and the sedimentation of particulates in the distal plume.

1. Introduction

The volcanic ash cloud that was generated by the eruption of Eyjafjallajökull in April 2010 caused considerable disruption to European airspace and international air travel. This provided a clear and well documented example of the importance of predicting the evolution of volcanic ash clouds. Forecasts of volcanic ash are provided by the Volcanic Ash Advisory Service with responsibility divided among different operational centres including the Met Office, UK. The Met Office's dispersion model, NAME (Numerical Atmospheric-dispersion Modelling Environment), is the operational model used (at the Met Office) for this purpose. In this paper we investigate the arrival of the ash cloud over the United Kingdom on 16th–18th April using ground-based lidar data and NAME simulations, with the aims of contributing to a better understanding of the processes that determine the location and concentration of the ash, assessing the ability of NAME to model the distal ash cloud, and understanding the sensitivities of the model results to various input parameters.

In this study, we focus on a quantitative comparison of the model with lidar data at two locations, Exeter (50.7°N, 3.53°W) and Cardington (52.1°N, 0.42°W), both in southern England (respectively in south-west and south-east England). We compare the vertically integrated concentration or column loading obtained from the model with the observed values. In the simulations presented here we use an estimate of the total mass emitted from the volcano and release this all as particles with a diameter of 100 μm or less. Because larger particles (both larger ash grains and composite particles formed through near-source aggregation) will fall out rapidly we expect to overpredict the column loads. However, the comparison between the model and observed values can be used to estimate the fallout of large particles near the volcano, although with significant levels of uncertainty. We also consider the ratio of the column loading to the maximum concentration in the vertical which gives an estimate of the typical layer thickness of the ash cloud. This enables us to estimate the extent to which NAME can resolve the observed thin layers. We also conduct simulations to investigate the sensitivity of the model results to a range of factors: the height of the eruption column, the source profile (the variation of source strength with height), 'turbulent diffusion' (representing the mixing by the unresolved eddies), and sedimentation. By assessing these sensitivities, we can gain some insight into the relative importance of these factors in

* Corresponding author.
E-mail address: ben.devenish@metoffice.gov.uk (B.J. Devenish).

1352-2310/$ – see front matter
doi:10.1016/j.atmosenv.2011.06.033

modelling the long-range dispersion of ash in the atmosphere. A complementary study, focussing on just 16th April but including some lidar data from Germany as well as from the United Kingdom, is presented by Dacre et al. (2011).

2. The NAME model

NAME is a Lagrangian stochastic model in which the trajectories of many model particles are followed through a realistic wind field which is usually provided by a Numerical Weather Prediction (NWP) model. As well as responding to the resolved flow field, the trajectories of the model particles contain a stochastic element which represents turbulent mixing by the unresolved eddies. Each particle carries a certain mass of the dispersing substance. When the substance consists of particulate material (as for volcanic ash), each model particle represents real particles (either individual grains or aggregates) of a certain diameter. The diameter remains fixed for the duration of the simulation (we thus ignore any agglomeration or break-up of aggregates during dispersion) and is drawn from a specified distribution. Sedimentation is treated by giving each particle a sedimentation velocity appropriate for its size. Particles are assumed to be spherical in shape with a Reynolds-number dependent drag coefficient (Maryon et al., 1999) and a slip flow 'Cunningham' correction factor (Pruppacher and Klett, 1997, p. 416) which becomes important for small particles. Dry deposition is treated using the resistance method to estimate a deposition velocity which is combined with the sedimentation velocity as described in Webster and Thomson (in press). Wet deposition is treated using washout coefficients (Maryon et al., 1999). For more details on NAME and its applications see Jones et al. (2007).

In the simulations to be presented below, the flow field is provided by the UK Met Office's NWP model, the Unified Model (UM). The global configuration of the UM is used with a horizontal grid spacing of about 25 km and 70 unequally spaced vertical levels extending into the mesosphere with a typical resolution of 300–400 m in the mid-troposphere. Flow field data were provided at three hourly intervals consisting of alternate analyses and short period forecasts.

Each model particle is treated as a solid particle with a density of 2300 kg m^{-3}. This may be an underestimate for some individual grains or an overestimate when the model particle represents an aggregate. However, the density and the particle size distribution together can be regarded as referring to the effective density and size needed to give the right sedimentation velocity. The height of the eruption column is estimated from radar measurements made by the Icelandic Meteorological Office (Arason et al., 2011). Unless otherwise stated, the model particles are released uniformly in the vertical between the volcano summit and the height of the eruption column with each particle carrying equal mass for a given mass release rate. There is no explicit modelling of the plume rise process itself with the model treating the ash as a passive, but sedimenting and depositing, tracer. The particle release rate is 200,000 h^{-1}. Tests showed that this produced results which were not unduly compromised by statistical noise. The simulation covers the period from the initial eruption on 14th April until 00:00 on 20th April 2010. The source strength is calculated according to the empirical relationship between the height of the eruption column above the volcano summit, z_{max}, and the mass emission rate, Q_m, given in Mastin et al. (2009):

$$Q_m = 140.876\, z_{max}^{4.15} \quad (1)$$

where z_{max} is measured in km and Q_m in kg s^{-1}. Note that, from Fig. 1 of Mastin et al. (2009), there is approximately a 50% chance that, for a given z_{max}, Q_m can differ from (1) by a factor of 3–4 or more. Equation (1) is similar to the relationship given by Sparks et al. (1997, Section 5.2) and the exponent, 4.15, is close to the value expected from dimensional analysis and integral plume models for vertically-rising plumes (Sparks et al., 1997, Section 2.6). Equation (1) takes no explicit account of the state of the atmosphere at the time of the eruption (such as the effects of atmospheric stability, wind speed and direction and ambient moisture) nor does it account explicitly for the effects of moisture at the source (such as the melting of the glacier above Eyjafjallajökull). Several studies (e.g. Woods, 1993; Bursik, 2001; Mastin, 2007; Tupper et al., 2009) have demonstrated that the state of the atmosphere can have a considerable effect on the height attained by the volcanic plume and that there may be significant departures from the empirical relationship given by (1) especially for weaker eruptions. Since the eruption occured below a glacier and was relatively weak, the effects of both moisture and the ambient wind are likely to give rise to potentially significant differences in the actual mass emission rate compared with the value given by (1). The evolution of the height of the eruption column and mass emission rate over the course of the simulation is shown in Table 1. The emission heights were determined subjectively to be at the upper end of the scatter seen in the 5-min radar values given by Arason et al. (2011), while not reflecting the most extreme values. During periods of little or no data the value prior to the period was retained.

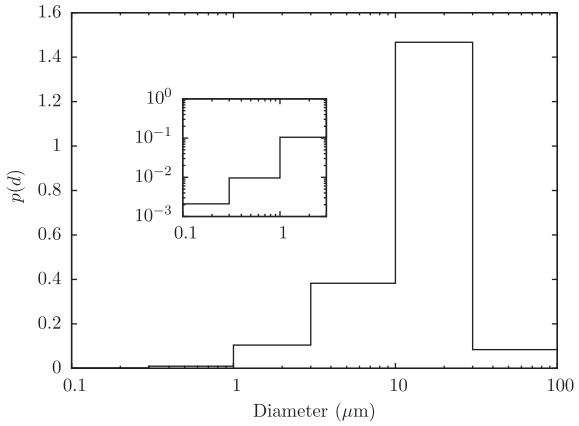

Fig. 1. The distribution of mass over different particle diameters. The area on the plot between any two diameters is proportional to the mass in this size range. The plot is normalised so that $\int p(d)\, d\log_{10} d = 1$. Inset: the range 0.1 μm ≤ d ≤ 3 μm in more detail.

All the emitted mass is distributed uniformly among the model particles with each model particle representing the mass of many real particles. For a given model particle, the real particles are all assumed to have the same diameter which is drawn from the probability distribution shown in Fig. 1.

Table 1
The evolution of the height of the eruption column above mean sea level, H, and the mass emission rate, Q_m, with time. The volcano summit height is taken to be 1666 m. Variations used in some simulations: (1) the height of the eruption column during the first time interval is reduced to 7.5 km and the corresponding emission rate becomes 2.126×10^5 kg s^{-1}; (2) the time interval is changed so that 16/04/2010 03:00 is replaced with 15/04/2010 12:00.

From	To	H (km)	Q_m (kg s^{-1})
14/04/2010 09:00	14/04/2010 19:00	9.0(1)	$5.495 \times 10^{5(1)}$
14/04/2010 19:00	15/04/2010 04:00	5.5	3.724×10^4
15/04/2010 04:00	16/04/2010 03:00(2)	6.0	6.193×10^4
16/04/2010 03:00(2)	18/04/2010 06:00	8.25	3.512×10^5
18/04/2010 06:00	18/04/2010 23:00	5.0	2.085×10^4
18/04/2010 23:00	19/04/2010 00:00	4.0	4.747×10^3

Within each bin log d is chosen from a uniform distribution over the appropriate range where d is the particle diameter. In reality, a large fraction of material is likely to be concentrated in particles with much larger diameters (either due to the intrinsic grain size or due to aggregation of grains into larger particles) but these particles fall out close to the source and so do not play a role in ash that travels far from the source. Of course, it would be possible to include these particles in the model but this would increase computational expense (since more model particles would be needed to produce reasonable statistics) and is still subject to a large degree of uncertainty regarding the size distribution. A more straightforward approach is to reduce the emission rate by a given factor to account for the near-source fallout. In this paper, though, we do not reduce the emission rate, instead we are interested in estimating the near-source fallout. By comparing the column loadings calculated from the model data with the observed values we can estimate the fraction of ash which is lost close to the source. We choose to base an estimate of the near-source fallout on the column loadings since these are not sensitive to the vertical averaging interval (either associated with explicit averaging or with limitations on what the model can resolve) as would be the case with concentrations.

The ash concentration is calculated by averaging over grid boxes that are approximately 40 km in each horizontal direction with a variety of values for the vertical grid box depth, dz, that vary from 100 m to 6000 m. Column loadings are calculated over the depth of the modelled atmosphere. Unless otherwise stated, all statistics are averaged over the hour preceding the stated time of the data. All times are UTC and all the model data are calculated with NAME III version 6.0.

3. Observations

Lidars are able to detect atmospheric aerosols and have excellent temporal and vertical resolution. In the absence of cloud, lidar data can be converted into an aerosol extinction coefficient (and its vertically integrated counterpart, aerosol optical depth) by solving the radiative transfer equation. Mass concentrations can then be estimated using a specific mass extinction cross-section which depends on the aerosol type and size. The presence of other aerosol complicates the retrieval process. However, ash can be distinguished from other aerosol by a strong signal in the depolorisation channel (Marenco and Hogan, 2011).

Ground-based lidar observations were carried out at Exeter on 16–18 April using a dual depolarisation Leosphere lidar as explained in Marenco and Hogan (2011). The method described therein was used to infer the vertically and temporally resolved ash extinction coefficient during the daytime. Unfortunately, as the ambient temperature drops below a certain threshold the cross-talk on the depolarisation channel is affected by a temperature-dependency which has not been successfully characterised. This prevents us from distinguishing night-time observations of the ash from other (primarily boundary-layer) aerosol and so the night-time data are not considered here. Ground-based lidar observations were also carried out at Cardington on 16 April using a similar lidar system. This system has not been characterised in terms of channel cross-talk and so we cannot use the method described in Marenco and Hogan (2011). However, on this day the ash layer was found to be distinct from the boundary-layer aerosol and therefore we use the method by Fernald (1984) and Klett (1985) and consider the ash to be the aerosol above 1500 m. The ash concentration at both locations was estimated from the measured ash extinction coefficient assuming a constant mass extinction cross-section of 0.6 $m^2\ g^{-1}$. This value of the mass extinction cross-section was estimated from particle size distributions measured at Chilbolton AERONET station (51.1°N, 1.4°W) on 16th April using a refractive index for desert dust and assuming the density of ash to be 2300 $kg\ m^{-3}$. Both Mie calculations and a non-spherical model gave similar values of the mass extinction cross-section. The error in this value was estimated to be of order a factor of two and this dominates the error (for concentrations that are not too small) leading to an uncertainty of order a factor of two in the concentrations. Further details of these calculations can be found in Johnson et al. (submitted for publication). All occasions with low cloud have been excluded from the data.

Fig. 2 shows the evolution of the ash cloud at Exeter as measured by the lidar on 16th, 17th and 18th April (Marenco and Hogan, 2011). The times shown in Fig. 2 correspond approximately to the hours of daylight. We note the following points about the observed concentrations: (i) no ash was detected before 13:00 on 16th April; (ii) occasions with low-level cloud have been removed from the data on 16th April which shows in Fig. 2a as gaps (vertical white stripes) in the plot; (iii) there is no missing data on 17th April; and (iv) the gap in the data around 18:00 on 18th April is due to cloud. We also make the following comments about the structure of the observed ash cloud: (a) the ash cloud on 16th April exhibits a sloping structure on the time–height plot; (b) there is little ash present on 17th April; (c) multiple layers are apparent on 18th April; and (d) the ash appears to reside primarily above the boundary layer on 16th April while some ash is mixed to the surface on the afternoon of 18th April.

Fig. 3 shows the temporal evolution of the column loading, maximum concentration and typical layer depth as measured by the lidar at Exeter. As with the contour plots in Fig. 2, we exclude any data between 20:00 and 07:00. Note how the column loading is higher on 18th April compared with 16th April whereas the reverse is true for the maximum concentration. As expected from Fig. 2 and demonstrated in Fig. 3c, this shows that the ash was concentrated

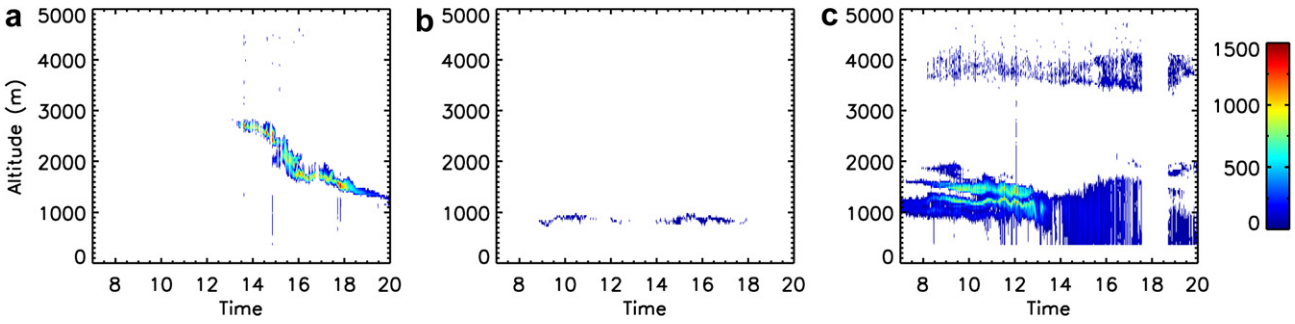

Fig. 2. The concentration of volcanic ash (in $\mu g\ m^{-3}$) at Exeter as measured by the lidar on (a) 16th, (b) 17th and (c) 18th April 2010. Any data larger than 1500 $\mu g\ m^{-3}$ is treated as 1500 $\mu g\ m^{-3}$ and any data less than 50 $\mu g\ m^{-3}$ is shown as white.

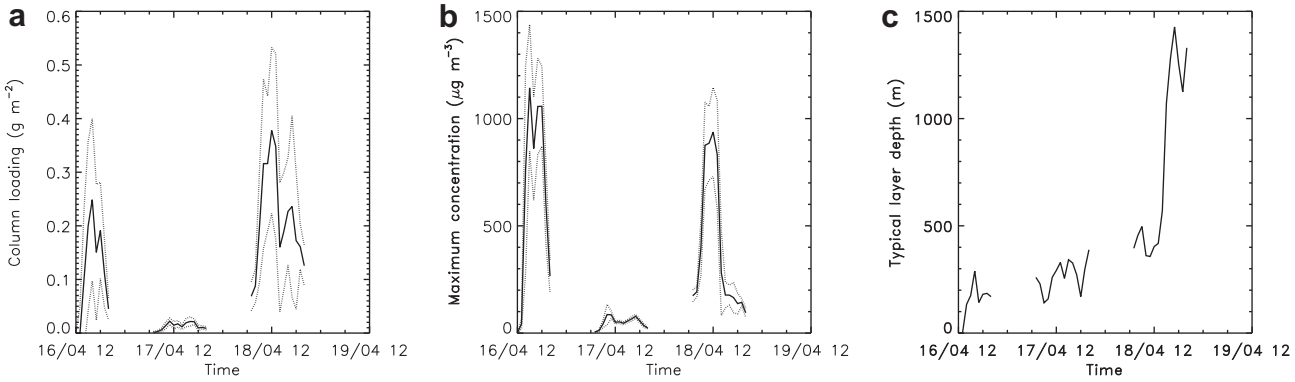

Fig. 3. The temporal evolution at Exeter of the observed (a) column loading, (b) maximum concentration and (c) typical layer depth. In figures (a) and (b) the solid line is the hourly averaged data and the dotted lines show the standard deviation of the 1-min values about this average. The height range 360 m–5000 m is used to calculate the data.

in thinner layers on 16th April but was more diffuse (thicker) on 18th April.

Fig. 4 shows a sloping ash cloud at Cardington on 16th April as measured by the lidar and closely resembling the observed ash cloud at Exeter. As discussed above, only ash above 1500 m is considered. There is no signal before about 07:00 (probably as a result of fog), no ash is detected between then and 08:00 or after about 13:00, and occasions with low-level cloud have been removed from the data between 08:00 and 13:00. Observations at Cardington on 17–18th April show very small amounts of ash and were not considered here. Lidar measurements from Chilbolton also show a similar sloping plume on 16th April (Dacre et al., 2011).

4. Comparison of NAME with lidar observations

Fig. 5 shows the evolution of the NAME ash cloud at Exeter from 15th to 19th April with the early part of the ash cloud (15–16th April) shown in more detail. The early part of the ash cloud shows a sloping structure with the cloud descending with time, consistent with the observations. However, there are some differences between the model and observations: the model ash cloud arrives approximately 12 h in advance of the lidar observation; on 15–16th April the model indicates the presence of ash between 3000 m and 6000 m (though at lower concentrations than below 3000 m) which is not detected by the lidar; and the depth of the model ash cloud is significantly larger than the observed depth indicating that NAME is not able to resolve the thin layers. After the early sloping part of the ash cloud NAME shows low-level ash on the 17th April which is joined by a higher layer on the 18th. This agrees qualitatively with the observations although the quantity of ash on the 17th is too large and that on the 18th is too small relative to the 16th. As on 16th the modelled ash layers are thicker than observed.

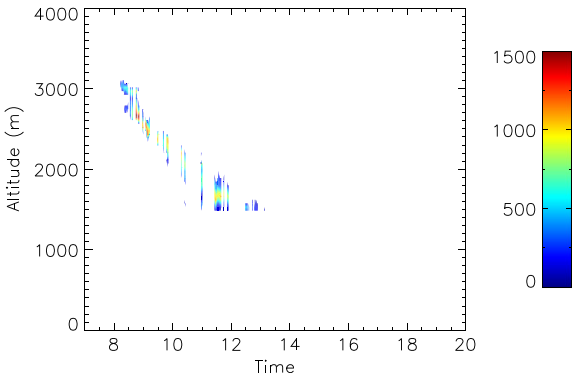

Fig. 4. As Fig. 2 but for the arrival of the ash cloud at Cardington on 16th April; only material above 1500 m is shown.

The early arrival of the ash in the model is perhaps the most significant of the differences and is also seen at Cardington (see Fig. 8 below) and at Chilbolton (Dacre et al., 2011). The general synopsis for 16th April shows easterly winds in southern England to the north of a weak cold front. Fig. 6 shows a horizontal contour plot of the modelled ash cloud over north-west Europe. It can be readily seen that the ash cloud splits into two branches with part of the ash cloud transported north-eastwards over Scandanavia and another part transported in a south-westerly direction over the UK, both parts travelling parallel to the cold front. Sensitivity tests involving the timing of the start of the eruption showed that the results at Exeter were insensitive to the release start time, with the material released at the start being carried into the north-east, and not the south-west, branch. At times before the arrival of material at Exeter and Cardington in the model, the branch of the cloud over the UK is modelled as extending rapidly to the west of Exeter and Cardington but to the north of these locations (not shown). It then arrives at these locations due to a slower southward movement of the branch. Assuming this modelled behaviour is correct, the timing error is not unexpected; a relatively small error in the branch's north–south position causes a large error in timing due to the slow southward movement. See Dacre et al. (2011) for further arguments supporting this view. The error in the north–south position and hence in the arrival time of the ash cloud could be due to errors in the height range over which material is emitted, errors in the dispersion modelling, and errors in the wind fields (including the errors caused by having winds available only every 3 h and linear interpolation in time). The sensitivity tests in Section 5 below go some way to eliminate the first two explanations leaving wind errors as the likely cause. However, it should be emphasised that the position error is small and not unexpected for material which has travelled a long distance, with errors accumulating along the way. Some of the other differences noted above will also be investigated using sensitivity tests in Section 5.

We will now consider quantitative comparisons between the model and the observations. Because the model predicts a sloping ash cloud in keeping with the observations yet significantly earlier than the observed ash cloud, we argue that any quantitative comparison should not be on a point-by-point basis in time: instead we compare peak values of the (hourly averaged) column loading and vertical maximum concentration.

Fig. 7a shows the evolution of the NAME column loading from 12:00 on 15th April to 12:00 on 19th April. After the arrival of the initial ash cloud (from approximately 16:00 on 16th April), the ash

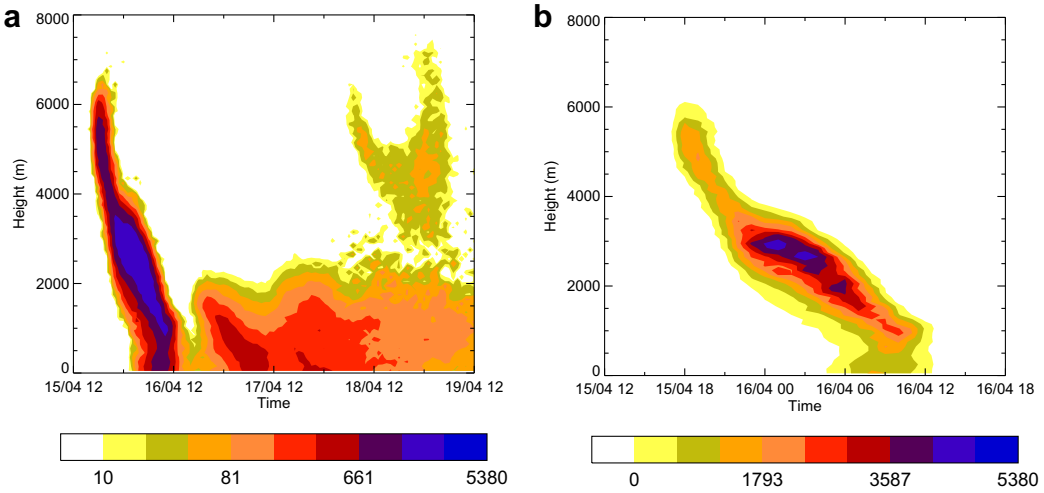

Fig. 5. The evolution of the NAME ash cloud at Exeter with $dz = 100$ m for (a) the total duration of the simulation and (b) 15–16th April in more detail. Concentrations are given in μg m^{-3} and the contours are logarithmically spaced in (a) and linearly spaced in (b).

persists at a relatively low concentration but, in contrast to the observations, there is no clear second peak of ash on 18th April. The initial peak value of the model column loading is 6.7 g m^{-2} which is approximately 27 times the peak value of the observed column loading, 0.25 g m^{-2}. The ratio of the model to observed column loading suggests that approximately 96.3% of the ash falls out close to the source due to processes not included in the model such as emission of material with large grain sizes or aggregation of small grains into large particles. We expect such processes to occur within a few 100 km of the source. We estimate that 3.7% survives into the distal ash cloud. It should be emphasised that this value is based on observations at a single location and so may not be representative of the whole ash cloud. There are further significant uncertainties in this figure due to uncertainties in the mass emitted, uncertainties in the observations and uncertainties in the modelling. The last of these uncertainties will be addressed to some extent by sensitivity tests below. However, because the value is substantially less than 100% it does indicate that the near-source fallout processes are significant and provides some indication of the magnitude of such processes. This level of near-source fallout is consistent with what has been observed for other eruptions elsewhere (Rose et al., 2000). For the second peak on 17th–18th April, the maximum observed value is 0.37 g m^{-2} compared with 1.1 g m^{-2} predicted by the model. This second ratio would indicate that a higher fraction of the ash particles survives into the distal plume than is the case in the early part of the plume. The possible reasons for this difference as well as the difference in the structure of the ash clouds will be discussed in Sections 5 and 6 below.

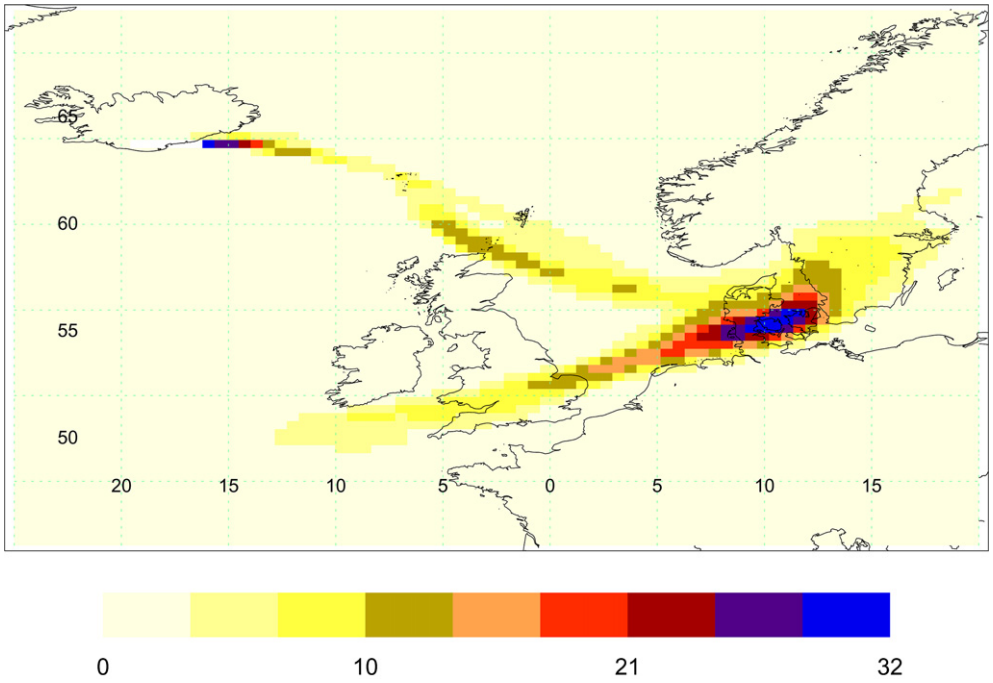

Fig. 6. Horizontal contour plot showing the NAME ash cloud over north-west Europe at 00:00 on 16th April 2010. The linearly spaced contours represent the column loading (g m^{-2}) which is calculated from data averaged over the preceding 3 h.

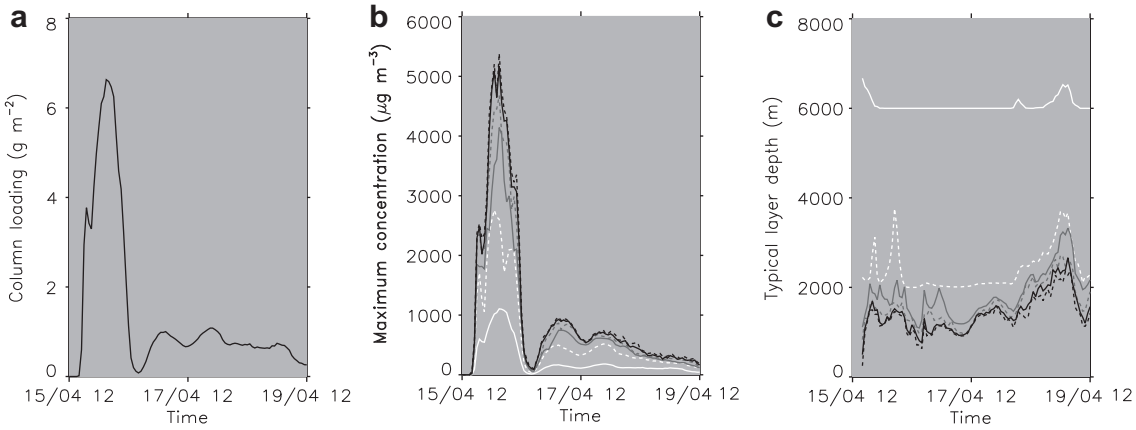

Fig. 7. (a) The evolution of the NAME column loading at Exeter; (b) the maximum concentration for different vertical resolutions: $dz = 6$ km (white-solid), $dz = 2$ km (white-dashed), $dz = 1$ km (grey-solid), $dz = 0.5$ km (grey-dashed), $dz = 0.2$ km (black-solid) and $dz = 0.1$ km (black-dashed); (c) the typical layer depth defined to be the ratio of the column loading to the maximum concentration for the same values of dz as used in (b).

Fig. 7b shows the evolution of the maximum concentration over the first 6000 m for dz ranging from 100 m to 6000 m. It shows that the maximum concentration may be considerably higher than the mean concentration over the first 6000 m consistent with the ash not being uniformly distributed over this layer (see Fig. 5). Fig. 7c shows that the typical layer depth reaches a minimum on 16th April and a maximum on 18th April, consistent with the thinner layers observed on 16th April and the more diffuse layers observed on 18th April. However, the depth of the modelled ash cloud even with $dz = 100$ m is still considerably larger than the depth of the observed ash cloud suggesting that NAME cannot resolve layers as thin as those observed by the lidar. NAME, being a Lagrangian model, has no intrinsic resolution limitation, but the resolution could still be limited by the resolution of the wind data, by the subgrid diffusion utilised in NAME, or by the diffuse vertical distribution of ash assumed at the source. The second and third of these possibilities are investigated below through tests of the sensitivity to the subgrid diffusion and to the source profile. The peak value of the maximum model concentration in the initial ash cloud at Exeter (15–16th April) is 5400 μg m^{-3} which is considerably higher than the largest values of the observed maximum concentration, although, because of the thicker model plume, not by as large a factor as the ratio of modelled to observed column loads. On 18th April, the observed and modelled maximum concentrations are comparable in magnitude.

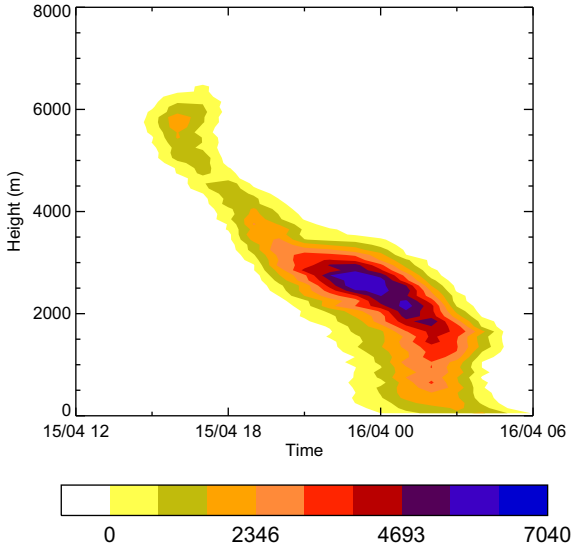

Fig. 8. The arrival of the NAME ash cloud at Cardington on 15–16th April. Concentrations are given in μg m^{-3} and the contours are linearly spaced.

The NAME model plume at Cardington is shown in Fig. 8. As at Exeter, the model plume arrives approximately 12 h in advance. The peak column loading predicted by the model at Cardington is 11.75 g m^{-2} compared with a peak value of the observed column loading of 0.17 g m^{-2}. This suggests that the near-source fallout is approximately 98.5% with 1.5% surviving into the distal plume. Although this differs from the value derived at Exeter for the early part of the ash cloud, the difference is within the expected level of uncertainty. The maximum concentrations and typical layer depths, both modelled and observed, are similar to those seen at Exeter with again the modelled values being larger than observed.

5. Sensitivity studies

In order to gain a better understanding of the physical processes which are important for the dispersion of ash in the atmosphere, we conduct a number of simulations to investigate the sensitivity of NAME to changes in (a) the height of the eruption column; (b) the vertical profile of the eruption column; (c) sedimentation; (d) vertical diffusion; and (e) horizontal meander. We illustrate the effects of these sensitivity studies with the results at Exeter; similar results were obtained at Cardington.

5.1. Height of the eruption column

Arason et al. (2011) quantify the error in the radar observations of the eruption column. They suggest that, near the start of the eruption on 14th April, a height of 7.5 km above mean sea level represents the mean eruption-column height over 6 h while 9 km (our original choice) corresponds to one standard deviation above the mean. Fig. 9b shows the evolution of the initial sloping ash cloud at Exeter for a simulation with a reduced eruption-column height of 7.5 km above msl from 09:00 to 19:00 on 14th April (variation 1 in Table 1). The maximum height of the ash cloud is clearly closer to what was observed by the lidar. Similarly, since the mass emission rate varies like $z_{\max}^{4.15}$, the model column loadings are smaller (see the results for 15–16th April in Fig. 10) suggesting a lower amount of near-source fallout.

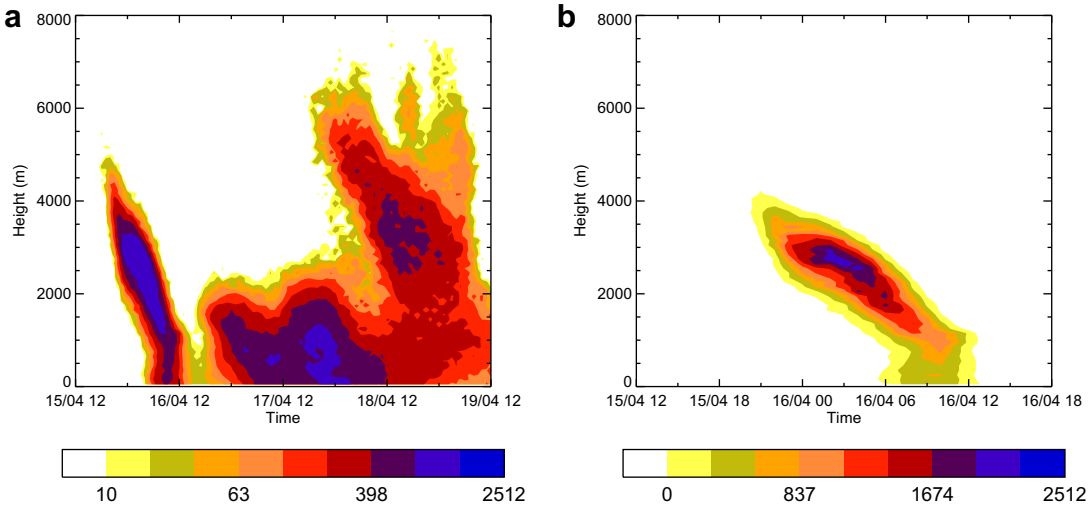

Fig. 9. As Fig. 5 but with the two changes to the eruption-column height described in Table 1. The second of these changes does not affect the initial ash cloud shown in figure (b).

The lack of a significant peak in the column loading on 18th April (see Fig. 7a) may also be related to uncertainties in the height of the eruption column. Analysis of the travel time for ash to reach observation sites at Chilbolton, UK and Leipzig, Germany (Dacre et al., 2011) showed that better agreement between the model and the observations could be achieved by increasing the height of the eruption column to approximately 8.25 km (above msl) from 12:00 on 15th April (variation 2 in Table 1). Such an increase may be admissible since the period between 12:00 on 15th April and 03:00 on 16th April corresponds approximately to a period when, for the most part, the ash cloud was obscured from the radar by precipitating clouds or the radar data was missing (see Arason et al., 2011). We conducted another simulation in which the eruption-column height is increased to 8.25 km (above msl) from 12:00 on 15th April. Fig. 10 shows the column loading with the revised eruption-column heights (variations 1 and 2 in Table 1). Compared with Fig. 7a there is a marked increase in the amount of ash reaching Exeter on 18th April. As before, the model predicts that the ash in the second peak (17th–18th April) grows both more rapidly and earlier than the observations. Comparing peak values of the column loading for the second peak we see that the model is 8.1 times as large as the observations suggesting that 12% of material reaches the distal plume.

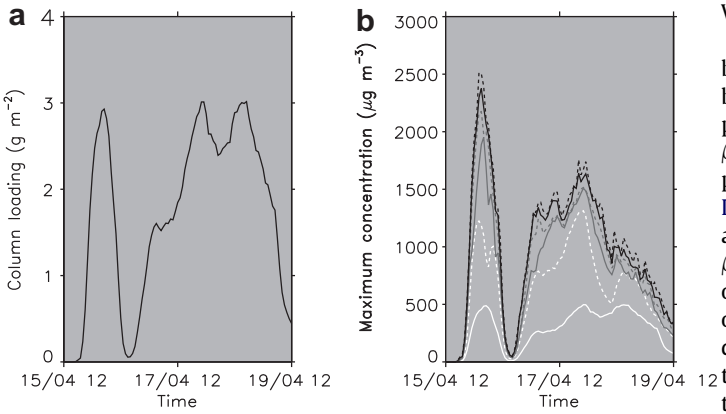

Fig. 10. As Fig. 7 but with the two changes to the eruption-column height described in Table 1: (a) column loading and (b) maximum concentration. The second of these changes does not affect the initial ash cloud.

Fig. 9a shows that the revised NAME simulation captures slightly more of the structure of the ash cloud shown by the observations on 17–18th April, particularly that, when the eruption-column height is increased to 8.25 km (above msl) from 12:00 on 15th April, there is more ash at higher elevations (circa 4000 m) on 18th April.

5.2. Vertical profile of the effective source

In the absence of a suitably strong crosswind, a volcanic plume typically forms a radially spreading umbrella cloud near the top of the eruption column (see e.g. Sparks et al., 1997, Section 11.2). Detrainment of material into the surrounding atmosphere occurs predominantly in this region. Observations of umbrella clouds suggest that its depth, Δz, is approximately $z_{max}/4$ with the height of the top and bottom of the umbrella cloud approximately coincident with respectively the maximum rise height of the eruption column and the level at which the eruption column first becomes neutrally buoyant. Since the lateral spreading of the umbrella cloud is most pronounced at the mid-point between the top and bottom of the umbrella cloud, where the density of the cloud equals that of the environment, the effective source profile of material can be modelled by a Gaussian distribution centred on this mid-point. The standard deviation of the Gaussian distribution is chosen to be equal to that of a uniform distribution over Δz, i.e. $\Delta z/\sqrt{12} = z_{max}/4\sqrt{12}$. We call this case the 'vertically-rising case'.

Relatively weak volcanic eruptions can be significantly distorted by the ambient wind. If the wind is sufficiently strong the plume becomes bent-over (so that its axis is horizontal). For a bent-over plume, the radius of the plume, b, at its maximum rise is given by βz_c, where β is the entrainment constant associated with bent-over plumes, which typically has a value in the range 0.4–0.6 (see e.g. Devenish et al., 2010), and z_c is the maximum height of the plume axis above the volcano summit (i.e. $z_{max} = z_c + b$). We choose $\beta = 0.5$ which gives $z_c = (2/3)z_{max}$ and hence the depth of the bent-over plume is $\Delta z = 2b = (2/3)z_{max}$. The spread of material in a bent-over plume about its axis can be approximated by a Gaussian distribution on a vertically orientated disc (although we only model the vertical profile and keep the horizontal source size as zero as for the other cases). We choose a standard deviation of $b/2 = \Delta z/4 = z_{max}/6$ so that it is equal to the standard deviation of a uniform distribution on a disc of radius b. We call this case the 'bent-over case'. The vertically-rising and bent-over cases represent the two

limiting cases of the effective source profile. The Eyjafjallajökull profile most likely lies somewhere in between, although the true profile may be more complex due to fluctuations in emissions associated with 'pulsing' of the eruption column.

Figs. 11 and 12 show the evolution of the ash cloud concentration profile, the column loading, the maximum concentration and the typical layer depth for both the vertically-rising and bent-over cases. Not surprisingly, the bent-over case more closely resembles, in its structure, the uniform line source since the standard deviation of the Gaussian distribution in the bent-over case is more than twice that of the vertically-rising case. In both cases the temporal peak of the column load and the vertical concentration maximum in the sloping ash cloud are approximately a factor of two larger than those from a uniform line source. On the other hand, the concentrations on 17–18th April show less sensitivity to the source profile. There is a larger gap (in time) between the sloping ash cloud on 16th April and the re-appearance of the ash cloud at Exeter on 17–18th April for the vertically-rising case compared with the bent-over case and, to an even greater extent, compared with the uniform case. This larger gap is more consistent with the lidar observations. Compared with the uniform case, the concentrations after this gap are a little larger and a little smaller for the bent-over and vertically-rising cases respectively. The layer depth for all three cases is similar suggesting that the depth of the plume at the source is not a significant factor in determining the plume thickness over Exeter.

The effect of a crosswind on a buoyant plume can be characterised by the dimensionless parameter $U/(z_{\max}N)$ where U is the wind speed and N is the buoyancy frequency (both assumed to be uniform with height; see e.g. Devenish et al., 2010; Sparks et al., 1997, Section 11.3). When $U/(z_{\max}N) \ll 1$, the effect of the crosswind is weak whereas $U/(z_{\max}N) \gg 1$ indicates that the crosswind is capable of bending the plume over. In reality, of course, the wind speed is not uniform with height and often exhibits significant vertical shear; we use the average wind speed over the height of the eruption column to obtain an order of magnitude estimate of $U/(z_{\max}N)$. The values of $U/(z_{\max}N)$ vary between 0.14 and 0.42 over the period 15–17th April. These values suggest that although the dynamics of the eruption column do not correspond to the bent-over plume limit, the wind did have a significant effect. Such an interpretation is consistent with the results of large-eddy simulations of buoyant plumes in a uniform crosswind (Devenish et al., 2010): for example, similar values of $U/(z_{\max}N)$ can be deduced from Fig. 11a of Devenish et al. (2010) (which shows the downwind evolution of the height of the centre

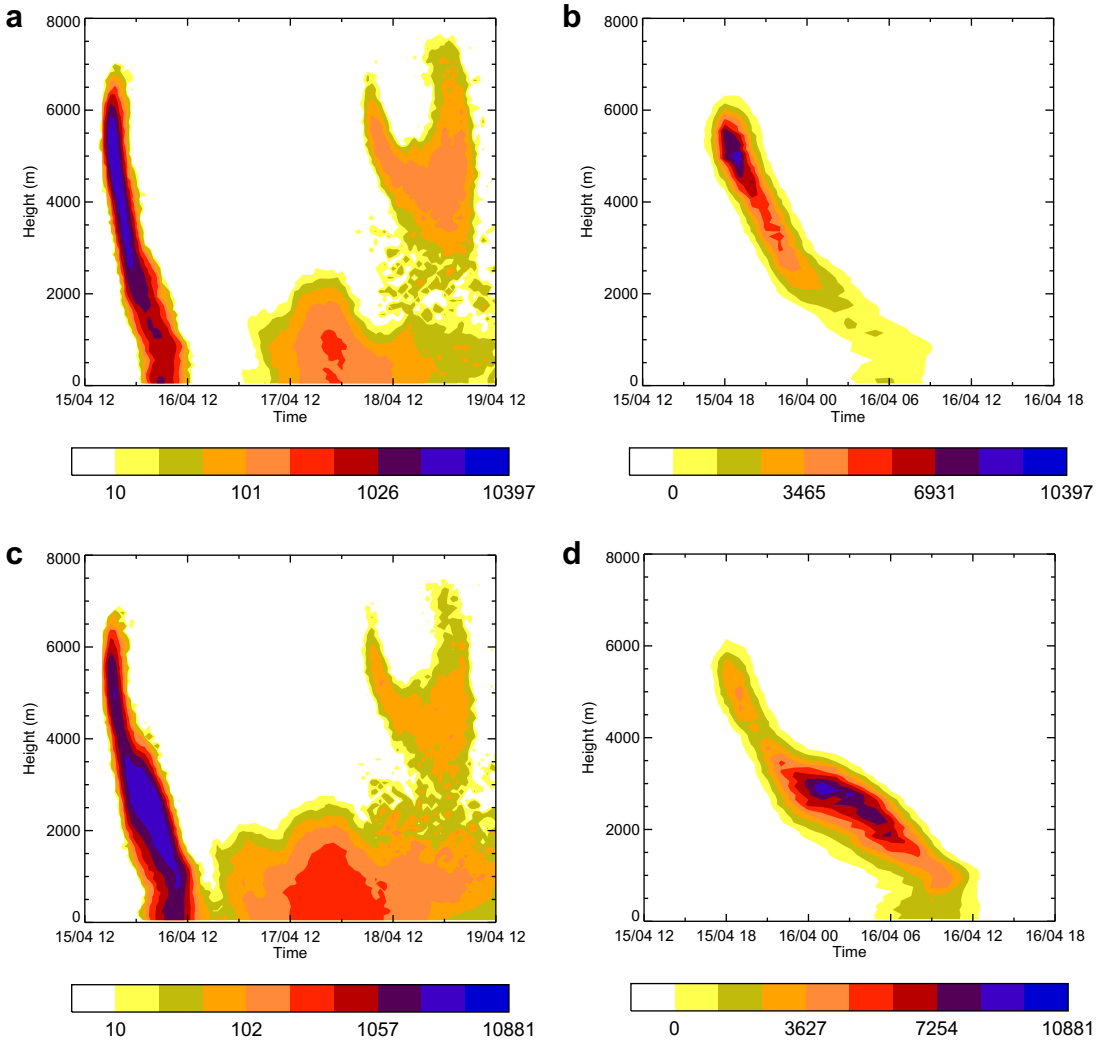

Fig. 11. As Fig. 5 but showing the evolution of the ash cloud at Exeter as generated by the Gaussian line source described in the Section 5.2: top row is the vertically-rising case and the bottom row is the bent-over case; the left-hand column shows the complete simulation with logarithmically spaced contours and the right-hand column shows the 15–16th April in more detail with linearly spaced contours.

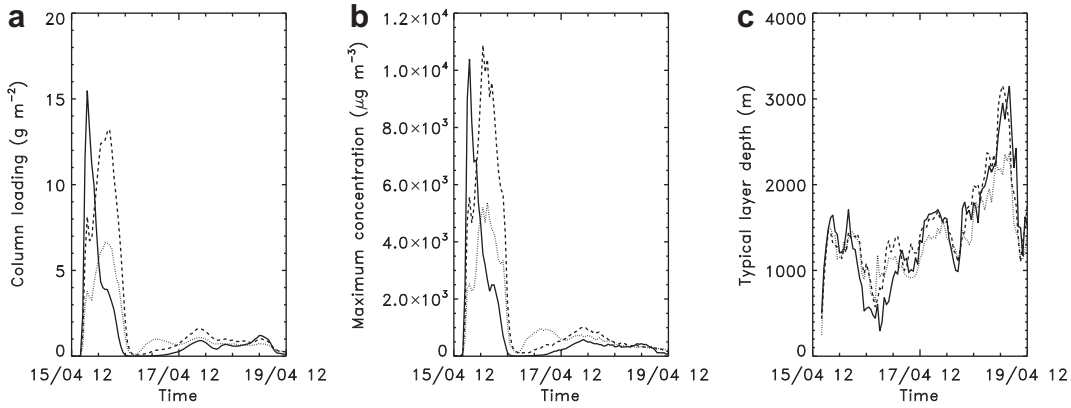

Fig. 12. The (a) column loading, (b) maximum concentration and (c) typical layer depth for $dz = 100$ m at Exeter from a vertical Gaussian line source: vertically-rising case (solid); bent-over case (dashed) and uniform source as in Fig. 7 (dotted).

of mass of the plume) for those plumes which rise close to the 45° line on this figure. These plumes are intermediate between the vertically-rising and bent-over cases.

It is possible that a Gaussian distribution of source material may concentrate material disproportionately around its centre, particularly as we are not accounting for the observed rapid fluctuations in the height of the eruption column (Arason et al., 2011). Thus, a distribution that does not decay as rapidly as a Gaussian may be more appropriate especially for the lower part of the eruption column.

5.3. Sedimentation

Fig. 13 shows the effect of neglecting the sedimentation of particles. We emphasise that we are not concerned here with the near-source fallout of large particles (a process which is not represented at all in our modelling) but with sedimentation in the distal plume. It is clear from Figs. 5a and 13 that the sloping nature of the initial ash cloud over Exeter is not primarily due to sedimentation. Since similar results hold for Cardington and Chilbolton (Dacre et al., 2011), it is likely that the ash cloud exhibits a slope in space (rather than time) which is advected over southern England. The slope will have evolved over the course of the ash cloud's trajectory from Iceland as a result of the non-uniform structure of the wind. Fig. 13 also indicates that much less ash reaches the ground on 16th April than in Fig. 5. However ash reaches the ground in significant quantities on 17–18th April even in the absence of sedimentation. Combined with the results of the elevated releases shown in Fig. 11 which also show ash at low levels on 17–18th April, this suggests that the ash that reaches low levels at Exeter on 18th April is due to subsidence i.e. the resolved-scale vertical velocity calculated by the UM.

5.4. Subgrid diffusion

As stated in Section 2, NAME includes a parameterisation of diffusion to account for turbulent mixing due to unresolved eddies. In addition to parameterising the effect of three-dimensional (3-D) turbulence, NAME also includes a parameterisation for the dispersive effects of lower frequency 'meandering' motions which are larger than the 3-D turbulence but which are not resolved by the input wind field from the UM. The meander applies only in the horizontal and has a much larger effect than the horizontal component of the 3-D turbulence. Model results without vertical diffusion, without horizontal meander and without both vertical diffusion and horizontal meander are shown in Figs. 14–16 respectively. The column loads, vertical maximum concentrations and layer depths are shown in Fig. 17.

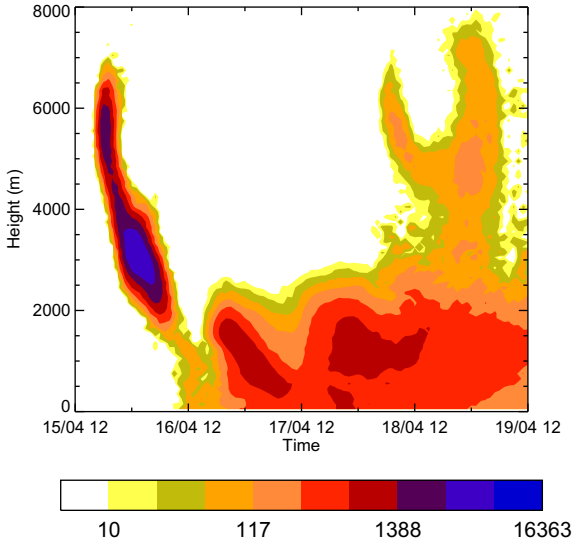

Fig. 13. As Fig. 5a but with no sedimentation.

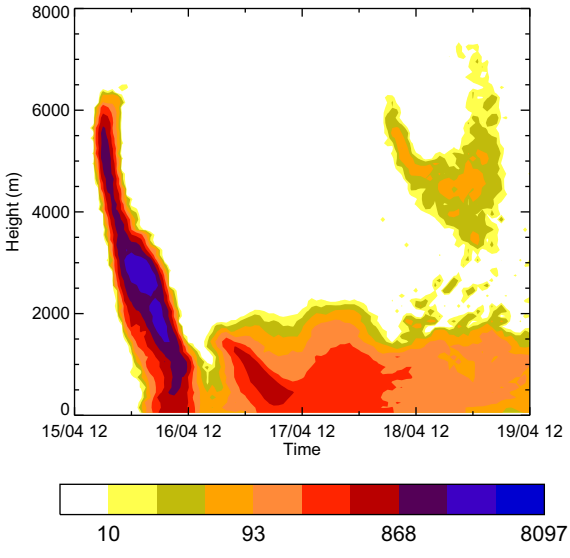

Fig. 14. As Fig. 5a but with no vertical diffusion.

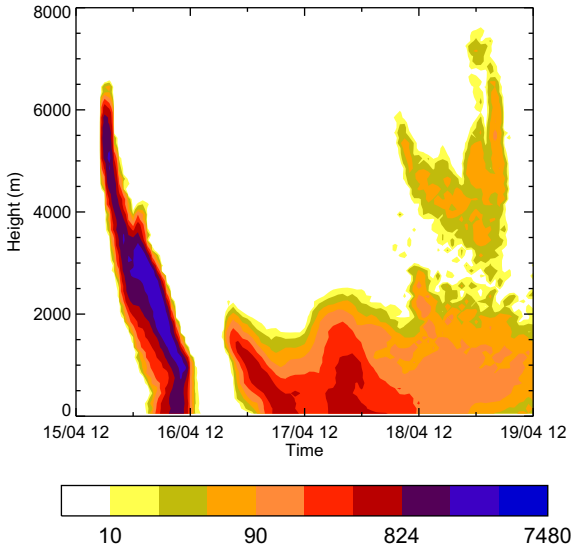

Fig. 15. As Fig. 5a but with no horizontal meander.

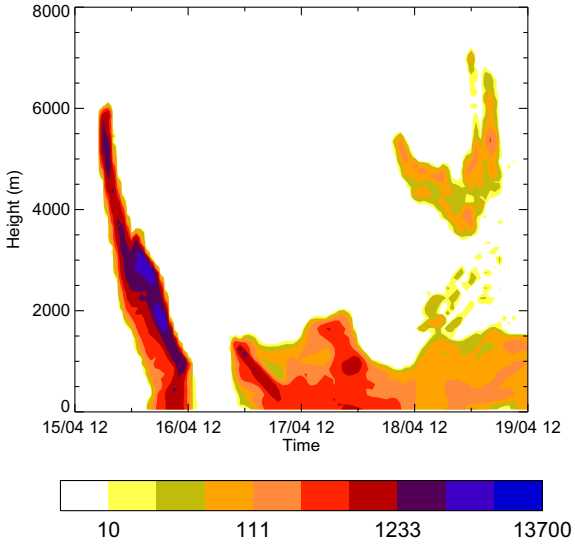

Fig. 16. As Fig. 5a but with no vertical diffusion or horizontal meander.

Since vertical diffusion acts to spread material in the vertical, we may expect the results of simulations without vertical diffusion to exhibit a narrower ash cloud with a higher concentration of material. The ash cloud in Fig. 14 is slightly thinner (in the vertical) than that in Fig. 5a (see also Fig. 17c) but still not as thin as the ash cloud observed by the lidar. The peak concentration is also somewhat higher than the peak concentration in Fig. 5 as one might expect with less diffusion. It is also worth noting that the layer of ash that occurs between 3000 m and 6000 m on 18th April is more detached from the layer close to the ground compared with Fig. 5. This also occurs when both vertical diffusion and horizontal meander are absent (see Fig. 16).

Fig. 15 shows that, without meander, the ash cloud is slightly thinner (in the vertical) compared with Fig. 5 (see also Fig. 17c). This is expected because extra horizontal diffusion (in the form of low frequency meandering motions) applied to a sloping layer will produce a deeper plume. As for the case without vertical diffusion, the peak concentration is higher than in Fig. 5. Note the larger gap compared with Figs. 5 and 14 between the initial ash cloud on 15–16th April and the re-appearance of the ash cloud on 17–18th April. This also occurs when both vertical diffusion and horizontal meander are absent (see Fig. 16).

Figs. 16 and 17c show that the combined effect of neglecting vertical diffusion and horizontal meander results in a thinner ash cloud than in Figs 5, 14 or 15 although still not as thin as the ash cloud observed by the lidar (except perhaps towards the end of the period of interest). Fig. 17a and b indicate that the maximum concentration increases significantly while the column loading is relatively unaffected by changes to the subgrid diffusion.

The results of these simulations without subgrid diffusion reveal the degree to which the dispersion of the ash cloud is dominated by the resolved scales. Overall, the results indicate that vertical diffusion and horizontal meander do not individually play a strong role in producing a deeper-than-observed ash cloud at Exeter. However taken together the resulting change is significant.

5.5. Combined sensitivities

In this section we describe the effect of combining some of the sensitivity tests described above. We first consider the combined effects of changes to the eruption-column height, as explained in Section 5.1, and changes to the source profile, as explained in Section 5.2. The column loadings, maximum concentrations and typical layer depths for these simulations are shown in Fig. 18. The

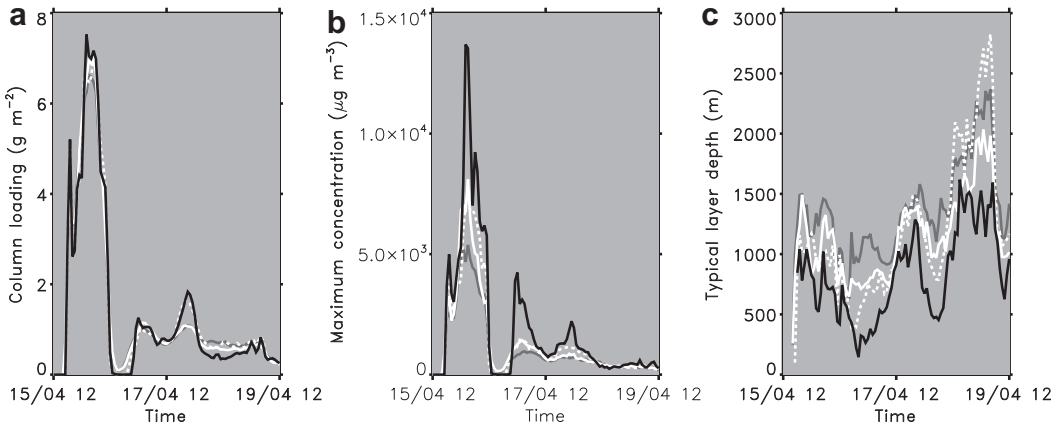

Fig. 17. The (a) column loading, (b) maximum concentration and (c) typical layer depth for $dz = 100$ m at Exeter for a uniform vertical line source: original simulation as in Fig. 7 (grey); no vertical diusion (white-solid); no horizontal meander (white-dashed); and no vertical diffusion or horizontal meander (black).

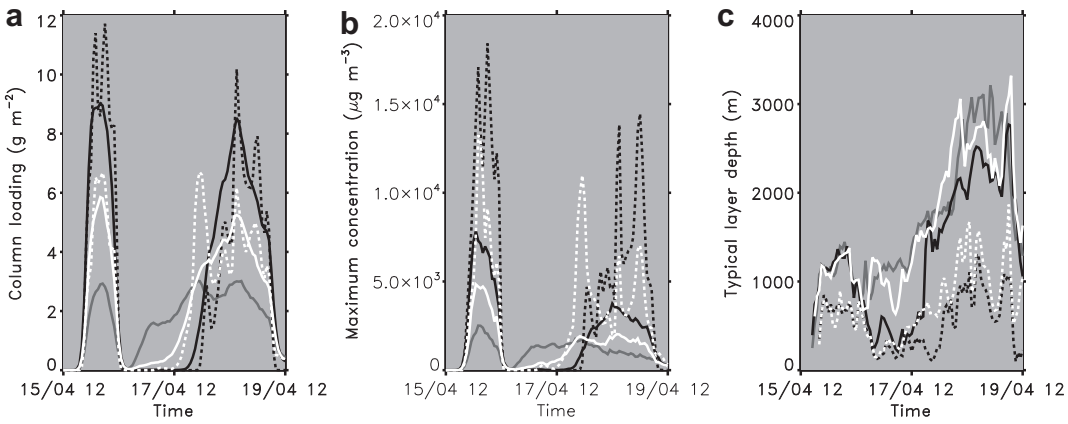

Fig. 18. The (a) column loading, (b) maximum concentration and (c) typical layer depth for $dz = 100$ m at Exeter for simulations with the revised eruption-column height as described in Table 1. The grey solid line represents the uniform source as in Fig. 10. The black lines represent the vertically rising case and the white lines the bent-over case. The solid and dashed lines respectively represent with and without subgrid diffusion (no vertical diffusion or horizontal meander).

differences in the column loading, maximum concentration and typical layer depth among the different source types in Fig. 18 are approximately the same as the differences in Fig. 12 except for the vertically-rising case which tends to show larger differences (relative to the uniform source) in Fig. 18. We also note that the latter case results in almost no ash on 17th April (not shown).

When these two simulations (revised eruption-column height with the two source profiles of Section 5.2) are repeated with no vertical diffusion or meander, we find that not only does the ash cloud become thinner (see Fig. 18c) but there is, in general, a significant increase in the column loading (shown in Fig. 18a) compared with the small differences in Fig. 17a. The vertical structure of the ash cloud is shown in Fig. 19: compared with the observations, it would appear that the bent-over case reproduces more of the structure of the ash cloud than the vertically-rising case suggesting that the ambient wind has a noticeable effect on the eruption column. In this context we remark that Webley et al. (2009) found a noticeable difference in some of their simulations of the 1992 Crater Peak (Mount Spurr) eruption in which the source was modelled either as an umbrella cloud or uniformly over the height of the eruption column. For that particular eruption, they noted that modelling the source as an umbrella cloud produced results which did not accurately show the distribution of the ash cloud at lower elevations and showed worse agreement with satellite data compared with the uniform source. It may simply be that the greater source depth of the bent-over case (in our simulations) or of the uniform source of Webley et al. (2009) better captures the rapid fluctuations of the eruption column which effectively produce a deeper source compared with the vertically-rising case. This may be especially true of the eruption of Eyjafjallajökull.

6. Discussion

The results of this study suggest that NAME captures many qualitative and quantitative aspects of the ash cloud generated by the eruption of Eyjafjallajökull in April 2010. In common with all models of the distal ash cloud which do not treat the near-source processes in detail and which use an effective source, NAME is sensitive to uncertainties in the effective source properties, namely emission rate, near-source fallout, vertical profile of emissions and particle size distribution. In addition the cumulative effect of small errors in the modelled meteorology along the trajectory of the ash cloud cause timing and positional errors common to all dispersion problems regardless of the source type; errors in the horizontal position of the ash cloud lead to errors in the column loading. In

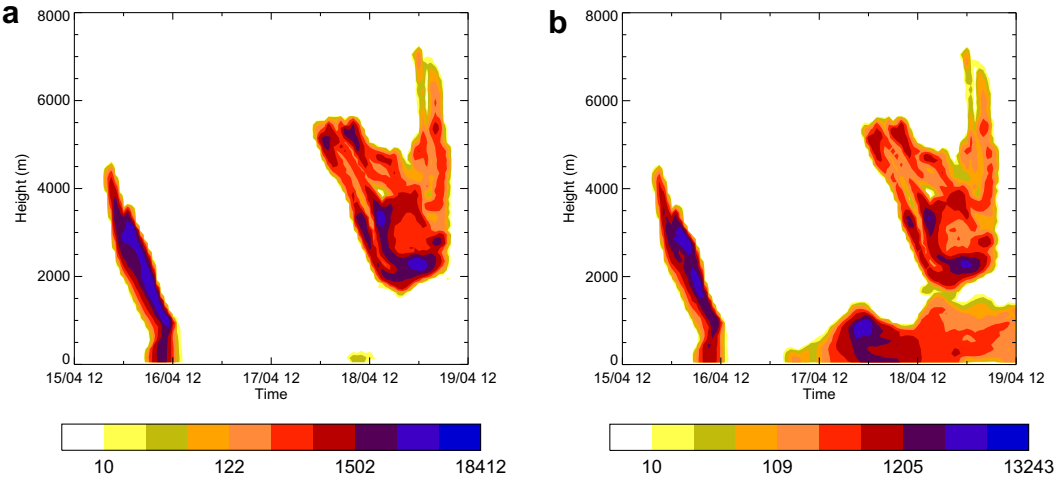

Fig. 19. As Fig. 5a but for the combined sensitivity tests described in Section 5.5: altered eruption-column height as in Table 1 and no vertical diffusion or horizontal meander for the (a) vertically-rising and (b) bent-over cases.

this context, it is not surprising that when all the sensitivities are taken into account we find a wide range of estimates of the near-source fallout (although consistent with previous estimates from other eruptions; Rose et al., 2000). However, it should be emphasised that these estimates are based on observations at two locations over four days and so may not be representative of the whole eruption. The fact that the ash cloud splits with part of the ash cloud transported north-eastwards over Scandinavia and another part transported south-westwards over southern England is likely to increase the difficulty of modelling the situation. The fraction of material transported in each direction may be sensitively dependent on the source position and height as well as the modelling of the structure of the wind field in the vicinity of the front. Without further information we are not in a position to assess whether the model has predicted these fractions correctly. More accurate estimates of the effective source properties might be possible if measurements were available within a few 100 km of the source but sufficiently far that near-source processes are no longer important (although this may not be possible for eruptions much larger than considered here as the near-source processes may take place over a much larger region).

Lidar observations over southern England (Fig. 3c) indicate an ash cloud of at most 1400 m in depth (as characterised by the ratio of column load to maximum concentration), and typically about 300 m, whereas the model ash cloud in Fig. 7c is in the range 1000–2000 m deep. Fig. 7 suggests that further increases in vertical resolution are unlikely to lead to a thinner ash cloud. As shown in Section 5.4, a reduction in the level of vertical diffusion and/or horizontal meander in the free troposphere leads to a thinner ash cloud but one which is still thicker than the narrow ash cloud observed by the lidar. It is possible that limited vertical resolution of the wind field (typically 300–400 m in the mid-troposphere) is responsible for the deeper-than-observed ash cloud. Another factor could be the role of density currents which are known to propagate over significant distances from large eruptions (see e.g. Sparks, 1986; Bursik et al., 1992; Sparks et al., 1997) and can lead to ash confined to narrow layers. However, the relatively small nature of this eruption along with the effect of the ambient wind would seem to militate against density currents playing an important role more than 1000 km downwind of the eruption. Indeed, Sparks (1986) has shown that the radial velocity of an umbrella cloud spreading from an eruption column reaching approximately 7 km into the atmosphere decreases from approximately 5 m s^{-1} close to the eruption column to less than 1 m s^{-1} at 10 km from the source. Despite the uncertainty in the physical processes leading to a narrow ash cloud, we may estimate the likely maximum concentration if NAME were able to resolve the ash cloud more accurately: if the depth of the ash cloud decreases by a factor of three, which would bring the depth of model ash cloud into line with the observed ash cloud, then we may expect the maximum concentration to increase by of order a factor of three. The difficulty in modelling the layer thicknesses means there is considerably more uncertainty in the maximum concentration than in the column loading.

The semi-empirical relationship between eruption-column height and mass emission rate derived by Mastin et al. (2009) and Sparks et al. (1997) takes no explicit account of the role of stratification, moisture or wind speed in either enhancing or reducing the height of the eruption column. It has been shown (see e.g. Sparks et al., 1997, Section 4.5.3; Woods, 1993; Mastin, 2007; Tupper et al., 2009) that entrained moisture can lead to a significant increase in the height of the eruption column primarily as a result of the additional energy provided by latent heating, although this is most likely to be important in the tropics. The eruption of Eyjafjallajökull in April 2010 occured beneath a glacier which is likely to have released a large amount of water vapour into the eruption column. Although this is different from entraining ambient atmospheric water vapour in that the melting/evaporation of the glacier will remove sensible heat, it is likely to lead to errors in estimating the mass emission rate from the eruption-column height alone. A strong crosswind can cause a relatively weak eruption column, such as that which emanated from Eyjafjallajökull in April 2010, to become bent-over (see e.g. Sparks et al., 1997, Section 11.3; Bursik, 2001) and not rise as high as might be expected for a given emission rate. Notwithstanding the difficulty in measuring the true maximum rise of the eruption column (which may be some distance downwind of the source in a strong crosswind), neglecting the effects of a crosswind could result in an underestimate of the mass emission rate from the eruption-column height alone. The use of an integral plume model to estimate the mass emission rate iteratively for a given atmospheric state and observed eruption-column height may help to reduce these uncertainties although they are likely to remain large.

The sensitivity tests outlined in Section 5 have provided some insight into the important parameters that govern long-range ash dispersion in the atmosphere. In particular, they have demonstrated the importance of accurate measurement of the source parameters such as the eruption-column height and the effective source profile but also the importance of the prescribed values of the vertical diffusion and horizontal meander. In addition the effective emission rate or, equivalently, the emission rate multiplied by the fraction that survives into the distal plume is of central importance. The results of this study point to the need to refine our ability to estimate these parameters.

Acknowledgements

We would like to thank Stephen Sparks and Sue Loughlin for helpful and informative discussions.

References

Arason, P., Petersen, G.N., Bjornsson, H., 2011. Observations of the altitude of the volcanic plume during the eruption of Eyjafjallajkull, April-May 2010. Earth System Science Data 3, 9–17.

Bursik, M.I., Carey, S.N., Sparks, R.S.J., 1992. A gravity current model for the May 18, 1980 Mount St. Helens plume. Geophysical Research Letters 19, 1663–1666.

Bursik, M.I., 2001. Effect of wind on the rise height of volcanic plumes. Geophysical Research Letters 28, 3621–3624.

Dacre, H.F., Grant, A.L.M., Hogan, R.J., Belcher, S.E., Thomson, D.J., Devenish, B.J., Marenco, F., Haywood, J.M., Ansmann, A., Mattis, I., 2011. Evaluating the structure and magnitude of the ash plume during the initial phase of the Eyjafjallajkull eruption using lidar observations and NAME simulations. Journal of Geophysical Research 116, D00U03, doi:10.1029/2011JD015608.

Devenish, B.J., Rooney, G.G., Webster, H.N., Thomson, D.J., 2010. The entrainment rate for buoyant plumes in a crossflow. Boundary-Layer Meteorology 134, 411–439.

Fernald, F.G., 1984. Analysis of atmospheric lidar observations: some comments. Applied Optics 23, 652–653.

Johnson, B., Turnbull, K., Dorsey, J., Baran, A., Ulanowski, Z., Cotton, R., Brown, P., Burgess, R., Capes, G., Webster, H.W., Haywood, J., In-situ observations of volcanic ash clouds from the FAAM aircraft during the eruption of Eyjafjallajökull in 2010. Journal of Geophysical Research, submitted for publication.

Jones, A., Thomson, D., Hort, M., Devenish, B., 2007. The UK Met Office's next-generation atmospheric dispersion model, NAME III. In: Borrego, C., Norman, A.-L. (Eds.), Air Pollution Modelling and its Application, vol. XVII. Springer, pp. 580–589.

Klett, J.D., 1985. Lidar inversion with variable backscatter/extinction ratios. Applied Optics 24, 1638–1643.

Marenco, F., Hogan, R.J., 2011. Determining the contribution of volcanic ash and boundary-layer aerosol in backscatter lidar returns: a three-component atmosphere approach. Journal of Geophysical Research, doi:10.1029/2010JD015415.

Maryon, R.H., Ryall, D.B., Malcolm, A.L., 1999. The NAME 4 Dispersion Model: Science Documentation. Met Office Turbulence and Diffusion Note 262. Available from. The National Meteorological Library, Exeter, UK.

Mastin, L.G., Guffanti, M., Servranckx, R., Webley, P., Barsotti, S., Dean, K., Durant, A., Ewert, J.W., Neri, A., Rose, W.I., Schneider, D., Siebert, L., Stunder, B., Swanson, G., Tupper, A., Volentik, A., Waythomas, C.F., 2009. A multidisciplinary effort to assign realistic source parameters to models of volcanic ash-cloud transport and dispersion during eruptions. Journal of Volcanology and Geothermal Research 186, 10–21.

Mastin, L.G., 2007. A user-friendly one-dimensional model for wet volcanic plumes. Geochemistry, Geophysics, Geosystems 8, Q03014.
Pruppacher, H.R., Klett, J.D., 1997. Microphysics of Clouds and Precipitation. Kluwer, Dordrecht, Netherlands.
Rose, W.I., Bluth, G.J.S., Ernst, G.G.J., 2000. Integrating retrievals of volcanic cloud characteristics from satellite remote sensors: a summary. Philosophical Transactions of the Royal Society A 358, 1585–1606.
Sparks, R.S.J., Bursik, M.I., Carey, S.N., Gilbert, J.S., Glaze, L.S., Sigurdsson, H., Woods, A.W., 1997. Volcanic Plumes. Wiley, Chichester, UK.
Sparks, R.S.J., 1986. The dimensions and dynamics of volcanic eruption columns. Bulletin of Volcanology 48, 3–15.
Tupper, A., Textor, C., Herzog, M., Graf, H.-F., Richards, M.S., 2009. Tall clouds from small eruptions: the sensitivity of eruption height and fine ash content to tropospheric instability. Natural Hazards 51, 375–401.
Webley, P.W., Stunder, B.J.B., Dean, K.G., 2009. Preliminary sensitivity study of eruption source parameters for operational volcanic ash cloud transport and dispersion models – a case study of the August 1992 eruption of the Crater Peak vent, Mount Spurr, Alaska. Journal of Volcanology and Geothermal Research 186, 108–119.
Webster, H.N., Thomson, D.J., Dry deposition modelling in a Lagrangian dispersion model. International Journal of Environment and Pollution, in press.
Woods, A.W., 1993. Moist convection and the injection of volcanic ash into the atmosphere. Journal of Geophysical Research 98, 17627–17636.